Characterization of cathodic arc deposited titanium aluminium nitride films prepared using plasma immersion ion implantation

2005 J. Phys.: Condens. Matter 17 2791

(http://iopscience.iop.org/0953-8984/17/17/029)

INSTITUTE OF PHYSICS PUBLISHING JOURNAL OF PHYSICS: CONDENSED MATTER

J. Phys.: Condens. Matter **17** (2005) 2791–2800 doi:10.1088/0953-8984/17/17/029

Characterization of cathodic arc deposited titanium aluminium nitride films prepared using plasma immersion ion implantation

S H N Lim[1,4], D G McCulloch[1], M M M Bilek[2], D R McKenzie[2], S P Russo[1], A S Barnard[3] and A Torpy[1]

[1] Applied Physics, School of Applied Sciences, RMIT University, GPO Box 2476V, Melbourne, Victoria 3001, Australia
[2] Department of Applied Physics, School of Physics (A28), University of Sydney, NSW 2006, Australia
[3] Center for Nanoscale Materials and Materials Science Division, Argonne National Laboratory, 9700 S Cass Avenue, Argonne, IL 60439, USA

E-mail: sunnie.lim@rmit.edu.au

Received 20 December 2004, in final form 13 March 2005
Published 15 April 2005
Online at stacks.iop.org/JPhysCM/17/2791

Abstract

This paper investigates thin films of titanium aluminium nitride grown using a stoichiometric metallic cathode in a cathodic arc vapour deposition system with plasma immersion ion implantation. The effect of various deposition conditions on the stress, microstructure and composition are evaluated. In general, the films were found to be both titanium and nitrogen rich. The application of voltages of 2 kV and greater was found to dramatically reduce the stress in the films. This stress reduction was found to be less pronounced at lower nitrogen flow rates due to a reduction in nitrogen implantation. The microstructure of the films was found to be cubic and at high voltages exhibited preferred orientation with {200} planes parallel to the surface of the film. We employ density functional theory to calculate the {100} and {111} surface energies and elastic constants for cubic titanium aluminium nitride. Using these calculated values, we explain this preferred orientation using a model which minimizes both surface energy and bulk strain energy.

1. Introduction

The ternary alloy titanium aluminium nitride (TiAlN) has been widely adopted as a high performance coating for tribological applications. This material has been shown to have several advantages over TiN for thin film coating applications [1–4]. For example, the indentation hardness of TiAlN coatings has been found to be higher than TiN coatings [2]. The coefficient

[4] Author to whom any correspondence should be addressed.

of friction is lower for TiAlN compared to TiN coatings at high sliding speeds [4]. One of the main disadvantages of TiN is that it can oxidize easily in air above 600 °C. TiAlN has a higher oxidation resistance compared to TiN, attributed to the formation of a protective aluminium oxide surface layer which inhibits oxygen diffusion [1, 2].

Intrinsic stress can limit the performance of coatings and is frequently observed in cathodic arc deposition as used for the coating of tools [5]. In this paper, we study the effect of ion bombardment during the growth of TiAlN by investigating stress, preferred orientation, structure and composition of films grown with plasma immersion ion implantation (PIII). The PIII process applies periodic high voltage pulses to the substrate which results in ion implantation of the growing film. In the case of TiN coatings, we have observed that the intrinsic stress can be reduced by approximately 50% by applying 2 kV pulses of a duration of 20 μs at a frequency of 500 Hz [6]. At the same time, the microstructure develops {200} preferred orientation as a result of the ion implantation [6–8]. To the best of our knowledge, no studies have been undertaken which investigate the effect of PIII on the structure and properties of TiAlN thin films. Here, we use electron microscopy, x-ray photoelectron spectroscopy (XPS) and stress measurements to investigate in detail the stress, microstructure and composition of TiAlN grown with PIII.

The development of preferred orientation in thin films grown under bombardment by energetic ions has been interpreted using several models. One class of models involves changes in the growth rate of crystallites of different orientations [9, 10]. Another class of models views the presence of channelling at high energies as a means of favouring the growth of crystallites which present open channels to the incoming beam and thus are not damaged by the high energy ion impacts [11, 12]. The third class of model compares the total energy of the growing film for different orientations and proposes that the system will develop the preferred orientation with the lowest total energy [13–15]. The TiAlN system provides another opportunity to compare the prediction of these models with experiments.

2. Experimental details

A cathodic arc deposition system equipped with PIII was used to fabricate TiAlN thin films on silicon wafer substrates with thickness between 330 and 350 μm. A stoichiometric TiAl alloy was used as a cathode. The PIII voltages, frequencies and the flow rate of nitrogen were varied systematically at constant nitrogen pressure of 1 mTorr while the microstructure and intrinsic stress were determined. The microstructure was examined by transmission electron microscopy (TEM) and diffraction.

Prior to deposition, the silicon substrate was chemically cleaned with acetone, then absolute ethanol and finally distilled water in an ultrasonic bath. This was followed by plasma cleaning (for 2 min) with nitrogen ions using a pulsing voltage of 10 kV and a flow rate of 40 sccm at a partial pressure of 1 mTorr. Each sample was deposited for 10 min and the pumping speed was adjusted to maintain a pressure of approximately 1 mTorr during deposition.

The residual stress in the coatings was determined by measuring the curvature of the samples using a Tencor surface profiler and applying Stoney's equation [16]

$$\sigma_{\mathrm{ave}} = \frac{E_{\mathrm{si}}}{6(1-\nu)} \frac{t_{\mathrm{s}}^2}{t_{\mathrm{f}}} \left(\frac{1}{r_{\mathrm{c}}} - \frac{1}{r_{\mathrm{u}}} \right) \tag{1}$$

where $\frac{E_{\mathrm{si}}}{6(1-\nu)}$ depends on the substrate elastic constants, E_{si} being the Young modulus of the substrate and ν being the Poisson ratio. For (100) silicon this constant, $\frac{E_{\mathrm{si}}}{6(1-\nu)}$, is 1.805×10^{11} N m^{-1}. The thickness of the substrate and film are t_{s} and t_{f} respectively. The parameters r_{c} and r_{u} are the radii of curvature of the coated and uncoated substrates respectively.

TEM samples were prepared in cross-section. Using a tripod polisher, the specimen was mechanically polished in the shape of a wedge. Further thinning was carried out using a Gatan ion beam thinner (model 600), and Gatan precision ion polisher system (model 691).

XPS was performed on a VG Microlab 310F using the Al Kα x ray source. TiN and AlN standards were used to determine the composition of the samples. For the TiN standard, the Ti 2p3 peak (centred at 454.8 eV) and N 1s peak (centred at 396.6 eV) were fitted with Gaussian–Lorentzian curves. A sensitivity factor γ_{TiN} was determined to be

$$\gamma_{\mathrm{TiN}} = \frac{[A_{\mathrm{Ti}}]_{\mathrm{TiN}}}{[A_{\mathrm{N}}]_{\mathrm{TiN}}}, \tag{2}$$

where A_{Ti} and A_{N} are the peak areas. Similarly, for the AlN standard the Al 2p peak (74.5 eV) and N 1s (296.4 eV) were used to obtain a sensitivity factor, γ_{AlN}, of

$$\gamma_{\mathrm{AlN}} = \frac{[A_{\mathrm{Al}}]_{\mathrm{AlN}}}{[A_{\mathrm{N}}]_{\mathrm{AlN}}}. \tag{3}$$

Inspection of the spectra showed that the two metallic species are not chemically bonded to each other, but rather to the nitrogen in the sample. In this work we adopt the notation $(\mathrm{Ti}_{1-y}\mathrm{Al}_y)_{1-x}\mathrm{N}_x$ to specify the composition of a titanium aluminium nitride film, therefore allowing both the ratios of metallic and metallic to nitrogen to vary, where x and y are between zero and unity. Using this approach x and y can be determined by

$$x = \frac{[A_{\mathrm{N}}]}{[A_{\mathrm{N}}] + \frac{[A_{\mathrm{Ti}}]}{\gamma_{\mathrm{TiN}}} + \frac{[A_{\mathrm{Al}}]}{\gamma_{\mathrm{AlN}}}} \tag{4}$$

and

$$y = \frac{\frac{[A_{\mathrm{Al}}]}{\gamma_{\mathrm{AlN}}}}{\frac{[A_{\mathrm{Ti}}]}{\gamma_{\mathrm{TiN}}} + \frac{[A_{\mathrm{Al}}]}{\gamma_{\mathrm{AlN}}}} \tag{5}$$

where $[A_{\mathrm{Ti}}]$, $[A_{\mathrm{Al}}]$ and $[A_{\mathrm{N}}]$ are the areas of the Ti 2p3, Al 2p and N 1s peaks respectively for the TiAlN alloy. By collecting spectra from three different regions of one of the films, the error in the concentration of nitrogen was found to be 5%.

3. Theoretical details

A $\mathrm{Ti}_{0.25}\mathrm{Al}_{0.25}\mathrm{N}_{0.50}$ structure was formed by replacing half of the metallic atoms in the rock-salt structure with a second metallic species, giving a structure of cubic symmetry in which each of the metal atoms has six second nearest neighbours of the same type and six of the opposite type. The c_{11}, c_{12} and c_{44} elastic constants for cubic $\mathrm{Ti}_{0.25}\mathrm{Al}_{0.25}\mathrm{N}_{0.50}$ were calculated using the periodic, linear combination of atomic orbitals (LCAO) formalism as implemented in the CRYSTAL03 package with the PBE GGA functional [17]. Here, the Bloch orbitals of the crystal are expanded using atom centred Gaussian orbitals with s, p or d symmetry. TiAlN was modelled as a 64-atom supercell using 86-411(d3), 85-11(d) and 7-311 basis sets for Ti, Al and N respectively. The Al and N basis sets were previously optimized and used in calculations of AlN [18]. Sampling of k-space has been performed using a Monkhorst–Pack mesh leading to a sampling of 150 k-points in the first Brillouin zone. The bulk modulus, B, was calculated by fitting the Murnaghan equation of state [19] to the computed energy–volume curve. The c_{11} and c_{44} elastic constants were computed by applying the relevant elastic strain tensor to the supercell [20] and fitting to the strain energy–deformation curve. The c_{12} elastic constant was obtained from the bulk modulus and c_{11} elastic constant using $B = (c_{11} + 2c_{12})/3$. The elastic compliances were obtained directly from the elastic constants.

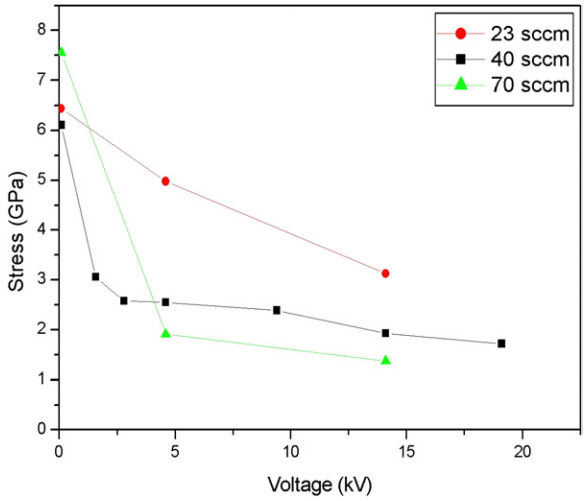

Figure 1. Residual stress as a function of the PIII applied voltage of the pulses for three different nitrogen flow rates. Here, the frequency was kept constant at 500 Hz.
(This figure is in colour only in the electronic version)

Surface energy calculations have been performed using the Vienna *Ab initio* Simulation Package (VASP) [21] within the framework of density functional theory (DFT) within the generalized-gradient approximation (GGA) with the exchange–correlation functional of Perdew and Wang (PW91 [22]). The atoms were represented using ultra-soft, gradient corrected Vanderbilt type pseudopotentials [23] as supplied by Kresse and Hafner [24] with outermost core radii of 2.79, 2.65 and 1.65 au for Ti, Al and N, respectively. The Fermi smearing method was used for the Brillouin zone integrations with a width of $\sigma = 0.2$ with a $5 \times 5 \times 5$ Monkhorst–Pack [25] k-point mesh.

The technique for calculating the surface energies used here is to subtract the bulk energy from the total energy of the slab, as the number of atoms approaches infinity, as given in [26]. In the present study, the {100} and {111} surfaces were generated by creating large slabs with eight and 12 atomic layers (192 and 288 atoms), respectively. Each structure was fully optimized (reconstructed) using valence orbitals expanding in a plane-wave basis up to a kinetic energy of 350 eV, whereas the final surface energies of the optimized structures were calculated with a cut-off of 500 eV (to improve accuracy), both to a convergence of 10^{-4} eV. All results were then corrected for the spin energies of 2.27, 0.189 and 3.26 eV for the Ti, Al and N atoms respectively and are in good agreement with the results of 2.24 and 3.11 eV for Ti and N calculated by Gall *et al* [27] using the PW91 functional, but with a cut-off of 350 eV.

4. Results and discussion

4.1. Intrinsic stress

Figure 1 shows the plot of the residual stress as a function of pulsing voltage for three different nitrogen flow rates (23, 40 and 70 sccm) at a pulse repetition rate of 500 Hz and pulse duration of 20 μs. As the pulsing voltage increases, the residual stress in the film decreases. Increasing the flow rate of nitrogen increases the efficiency of the stress relief process (see figure 1). A decrease in the stress of the film by approximately 50% compared to a film prepared without PIII was observed for pulsing voltages of 2–5 kV with nitrogen flow rates of 40 and 70 sccm.

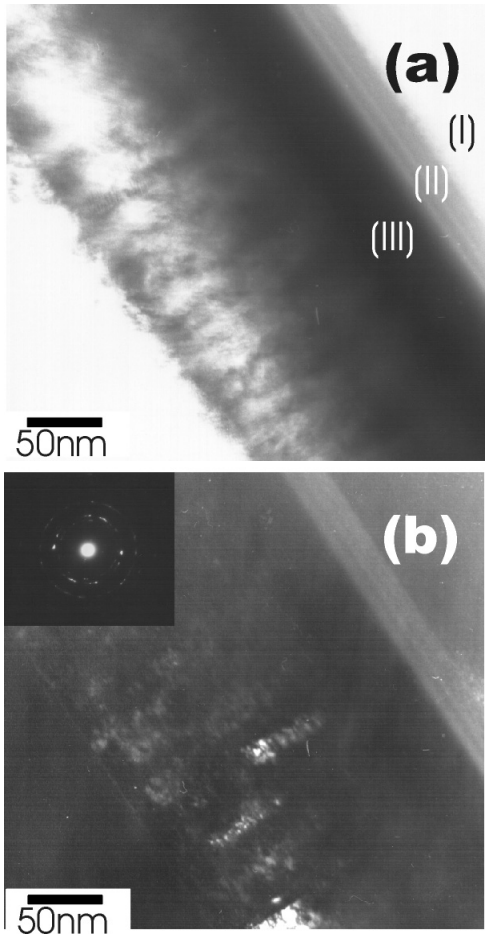

Figure 2. (a) TEM bright-field image, (I) Si substrate, (II) mixing layer, (III) TiAlN film; (b) dark-field image from the {200} reflection from a sample prepared without PIII and a nitrogen flow rate of 40 sccm. A typical diffraction pattern from the film is also shown as the inset in (b).

A similar level of stress reduction was observed in the case of TiN films and can be explained by the ion bombardment during film growth [28]. Ion impacts generate thermal spikes which increase the mobility of atoms within the growing film and allow them to rearrange into more energetically favourable positions [29], relieving intrinsic stress. The stress reduction is less in the case of the lower nitrogen flow rate due to a reduction in nitrogen ions available for implantation.

4.2. Microstructure and composition

Figure 2(a) shows the bright-field image of a sample prepared without PIII using a flow rate of 40 sccm. The thickness of the coating is approximately 210 nm. The diffraction pattern of this region shows little evidence of preferred orientation; however, the {200} reflections are the most prevalent. Figure 2(b) shows a dark-field image from a {200} reflection and reveals that the crystallites are small and columnar in morphology. These columnar crystallites extend across a substantial fraction of the film. The amorphous region created in the Si substrate during the initial nitrogen ion bombardment is evident in the bright-field image at the film/substrate interface. TEM was also performed on a sample prepared without PIII with the flow rate of 23 sccm and was found to have similar morphology.

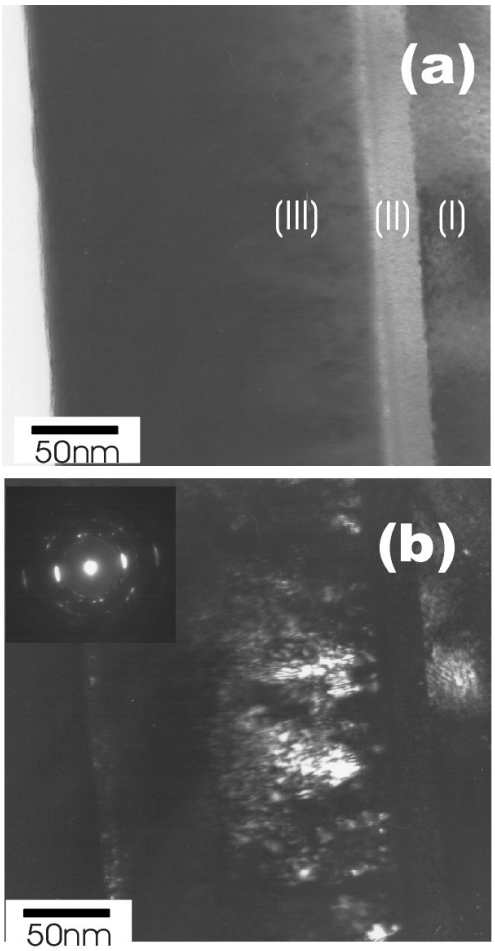

Figure 3. (a) Bright-field image, (I) Si substrate, (II) mixing layer, (III) TiAlN film; (b) dark-field image from the {200} reflection for a sample prepared using 14.1 kV pulsing voltage with a frequency of 500 Hz, a pulse length of 20 μs and a nitrogen flow rate of 40 sccm. A typical diffraction pattern from the film is also shown as the inset in (b).

Figures 3(a) and (b) are bright-field and dark-field images respectively for a sample prepared using 14.1 kV pulsing voltage with a frequency of 500 Hz and a pulse length of 20 μs, with a nitrogen flow rate of 40 sccm and a partial pressure of approximately 1 mTorr during deposition. The film thickness of this sample is approximately 190 nm. The corresponding diffraction pattern shows a very strong preferred orientation in the {200} planes, which are aligned perpendicular to the substrate. Dark-field images obtained from the {200} reflections do not reveal the columnar structure characteristic of the previous sample. {200} preferred orientation was also observed for a sample prepared using a 4.6 kV pulsing voltage.

TiAlN can exhibit two basic crystal symmetries: the cubic structure at small y, where it resembles TiN, and the hexagonal structure at large y, which resembles AlN. The transition between the cubic phase and the hexagonal phase occurs when the concentration of Al is between 52 and 67% [30–33]. The crystal symmetry of the samples is determined from the diffraction pattern obtained from TEM analysis. By measuring the diameter of the rings, their ratios can then be compared to the expected ratio for a cubic structure. The diffraction pattern obtained from a sample of composition $Ti_{0.22}Al_{0.20}N_{0.58}$ prepared without PIII is shown in figure 4. The first four rings of this diffraction pattern are indexed to cubic TiAlN. Table 1 shows the ratios of the diameters of the first four rings to the diameter of the first ring and it

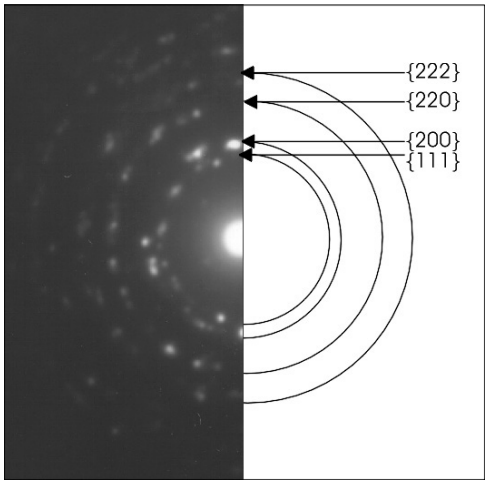

Figure 4. Diffraction pattern of a $Ti_{0.22}Al_{0.20}N_{0.58}$ prepared without PIII indexed assuming a cubic structure.

Table 1. Comparison of the ratio of the diameter of diffraction rings as measured from a diffraction pattern with that expected for cubic $Ti_{0.25}Al_{0.25}N_{0.50}$.

Ring (R)	Experimental ratio (d_1/d_R)	Calculated ratio
1	1.000	$d_{\{111\}}/d_{\{111\}} = 1.000$
2	0.857	$d_{\{111\}}/d_{\{200\}} = 0.866$
3	0.625	$d_{\{111\}}/d_{\{220\}} = 0.612$
4	0.517	$d_{\{111\}}/d_{\{222\}} = 0.500$

Table 2. Summary of the compositions for selected $(Ti_{1-y}Al_y)_{1-x}N_x$ samples obtained from XPS.

Flow rate (sccm)[a]		Pulsing voltage (kV)		Frequency (Hz)	
23	$Ti_{0.21}Al_{0.19}N_{0.60}$	0	$Ti_{0.22}Al_{0.20}N_{0.58}$	100	$Ti_{0.25}Al_{0.19}N_{0.56}$
40	$Ti_{0.22}Al_{0.20}N_{0.58}$	4.5	$Ti_{0.25}Al_{0.19}N_{0.56}$	500	$Ti_{0.25}Al_{0.19}N_{0.56}$
70	$Ti_{0.26}Al_{0.20}N_{0.54}$	14.1	$Ti_{0.28}Al_{0.24}N_{0.48}$	1000	$Ti_{0.25}Al_{0.21}N_{0.54}$

[a] Note that these samples were prepared without the assistance of PIII.

can be seen that they correspond very accurately to {111}, {200}, {220} and {222} reflections of the cubic TiAlN phase.

XPS analysis was used to observe the chemical composition variations with flow rate of nitrogen, pulsing voltage and the frequency of the pulses. Table 2 summarizes the results obtained from this compositional analysis. The application of PIII was not used while varying the nitrogen flow rate. The content of nitrogen increased when the flow rate was increased from 23 to 40 sccm as a result of the additional nitrogen present. However, the change in the flow from 40 to 70 sccm while maintaining a partial pressure of 1 mTorr appears to decrease the nitrogen content slightly. A 'saturation amount' of nitrogen appears to be reached. This effect may be due a reduction in the residence time of the nitrogen atoms in the chamber with increasing flow rate resulting in a decrease in the number of nitrogen ionization events.

The effect of varying the pulsing voltage on the composition was examined while keeping the flow rate of nitrogen at 40 sccm and the frequency of pulsing at 500 Hz. A decrease in the concentration of nitrogen was observed as the voltage increases, possibly because of preferential sputtering of nitrogen by nitrogen. The chemical composition remains unaltered when the frequency of the pulses is varied.

4.3. Surface morphology and termination

Jiang *et al* [34] have observed that {111} oriented TiN films consist of {111} columns terminated with {100} facets. The surface free energy $S_{\{111\}(\text{facet})}$ is defined as the energy per unit area of film for a TiN film with {111} columns having {100} facets. This quantity is calculated using the following expression:

$$S_{\{111\}(\text{facet})} = AS_{\{100\}}. \tag{6}$$

Here, A is the geometrical factor giving the additional surface area of a {111} oriented film because of its termination in {100} facets. For a cubic structure, A is $\frac{3}{2}\sqrt{3}$. The average surface energies calculated by Marlo and Milman [26] for the {100} and {111} surfaces of TiN are 1.21 and 4.82 J m^{-2} respectively. This gives a value of $S_{\{111\}(\text{facet})}$ of 3.14 J m^{-2} so that the {100} termination for a {111} oriented columnar TiN film is more energetically favourable than a {111} termination of each column. This agrees with experimental observation [34].

We have calculated the surface energy for the {100} and {111} orientations for $Ti_{0.25}Al_{0.25}N_{0.50}$. The surface energy $S_{\{100\}}$ is 0.62 J m^{-2} and the value of $S_{\{111\}}$ is 1.53 J m^{-2}. This gives the value of $S_{\{111\}(\text{facet})}$ of 1.60 J m^{-2} so that we expect that, unlike TiN, $Ti_{0.25}Al_{0.25}N_{0.50}$ {111} oriented films should terminate in {111} facets, but because the values are much closer than those for TiN the conclusion is more strongly dependent on the accuracy of the calculated surface energy.

4.4. Energy minimization model

The energy minimization model [6, 14] predicts that for cubic TiAlN the difference in energy per unit area ΔE between {111} and {100} oriented films can be expressed as

$$\Delta E = \Delta G \cdot t + \Delta E_{\text{surf}}. \tag{7}$$

Here, t is the thickness of the film, ΔE_{surf} is the difference in energy of the free surface between the two orientations and ΔG is the difference in the bulk strain energy per unit volume between the {111} and the {100} and is given by

$$\Delta G = G_{111} - G_{100} = \frac{\sigma^2(s_{11} - s_{12} - \frac{1}{2}s_{44})}{3}, \tag{8}$$

where s_{11}, s_{12} and s_{44} are the elastic compliances for cubic $Ti_{0.25}Al_{0.25}N_{0.50}$ and σ is the magnitude of the stress.

To the best of the author's knowledge, there have been no published experimental elastic constant values or free surface energies for $Ti_{0.25}Al_{0.25}N_{0.50}$. However, Chen [35] has calculated the elastic compliance values for $Ti_{0.375}Al_{0.125}N_{0.50}$ using density functional theory. The elastic compliance values that we have calculated for $Ti_{0.25}Al_{0.25}N_{0.50}$ are similar to the values of Chen as shown in table 3.

Figure 5 shows plots of ΔE versus stress calculated using our elastic compliance values for a range of film thicknesses. The films studied using TEM are indicated on the figure as circles (samples A–D) and lie in the region of the diagram where the lowest energy orientation is {100}. This is in agreement with our TEM analysis, as we have only seen {100} oriented films. It is expected that preferred orientation will be strongest in the two samples prepared using PIII which have a lower stress (samples A and B). Vlasveld *et al* [5] have observed that thick and highly stressed coatings of cubic TiAlN are {111} oriented. The intrinsic stresses of these coatings varied from 7.67 to 11.81 GPa for thicknesses between 900 nm and 1.2 μm. We have also plotted the data of Vlasveld *et al* in figure 5 with squares. The model predicts that the films of Vlasveld *et al* should all be {111} oriented in agreement with the experimental observations.

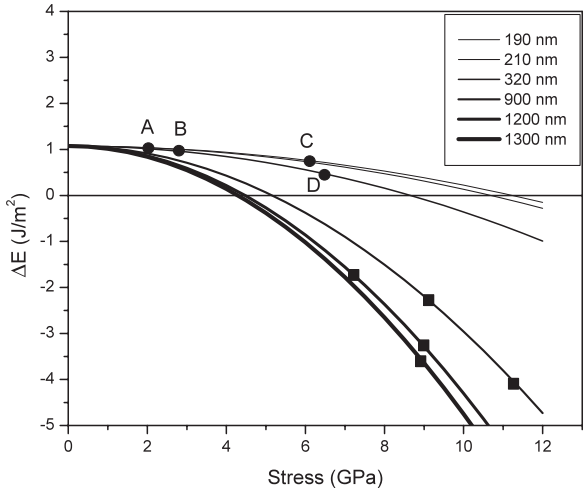

Figure 5. Plots of ΔE versus stress calculated using our elastic compliance values for a range of film thicknesses for $Ti_{0.25}Al_{0.25}N_{0.50}$ thin films. Also shown are several of our films (circles) and the films of Vlasveld *et al* [5] (squares). Samples A and B were deposited with the frequency of 500 Hz, flow rate of 40 sccm and voltages of 14.1 and 4.6 kV respectively. Samples C and D were prepared without PIII at flow rates of 40 and 23 sccm respectively.

Table 3. Comparison of the elastic compliances for $Ti_{0.375}Al_{0.125}N_{0.50}$ calculated by Chen [34] and the elastic compliances for $Ti_{0.25}Al_{0.25}N_{0.50}$ calculated in our work.

Elastic compliance	$Ti_{0.375}Al_{0.125}N_{0.50}$	$Ti_{0.25}Al_{0.25}N_{0.50}$
s_{11}	2.27×10^{-3}	2.15×10^{-3}
s_{12}	-5.02×10^{-4}	-4.25×10^{-4}
s_{44}	5.75×10^{-3}	5.41×10^{-3}

The channelling model states that the preferred orientation in a thin film grown with ion bombardment is the one that presents open channels to the incoming ion beam. This could arise, for example, from the destruction of seed crystallites presenting closed directions to the incoming beam. We cannot differentiate between the channelling model and the energy minimization model discussed above using the data at hand since both models predict the same orientation at high ion energies. However, of the two models, only the energy minimization model predicts a thickness dependence of the preferred orientation. A reversal of orientation with film thickness is consistent with the energy minimization model and was also observed in the case of TiN [6].

5. Conclusion

In this paper we investigated the stress, structure and chemical composition of TiAlN films deposited in a filtered cathodic arc with PIII. By applying pulsing voltages of between 2 and 5 kV and higher, we observed a decrease of approximately 50% in the stress as compared with films deposited without PIII. This stress reduction, due to ion bombardment during film growth, is less effective at low nitrogen flow rates. Analysis of the chemical composition using XPS showed that the samples were generally both Ti and N rich compared to that expected for stoichiometric $Ti_{0.25}Al_{0.25}N_{0.50}$ films. The films were found to have a cubic structure consistent

with previous observations that found that Ti rich coatings of TiAlN are cubic. Applying an energy minimization model which takes into account both surface energies and elastic stain energies in the TiAlN system, we were able to explain the {100} preferred orientation observed in our low stress films prepared at higher pulsing voltages. This model was also used to explain the {111} preferred orientation which has been observed by other researchers in the case of thick and highly stressed films.

Acknowledgments

The authors wish to acknowledge Dr B Latalla from ANSTO for some of the discussions relating to hardness measurements results, Dr J du Plessis from RMIT University, Applied Physics for his help with some of the interpretations of the XPS results and some useful feedback from Dr A Anders from Lawrence Berkeley National Laboratory. A S Barnard would like to acknowledge support, in part by the US Department of Energy, Office of Basic Energy Sciences, under contract No W-31-109-ENG-380.

References

[1] Chakrabarti K, Jeong J J, Hwang S K, Yoo Y C and Lee C M 2002 *Thin Solid Films* **406** 159
[2] Kim K and Lee S 1996 *Thin Solid Films* **283** 165
[3] Cheng Y H, Tay B K, Lau S P, Shi X and Chua H C 2000 *Thin Solid Films* **379** 76
[4] Yoon S Y, Kim J K and Kim K H 2002 *Surf. Coat. Technol.* **161** 237
[5] Vlasveld A C, Harris S G, Doyle E D, Lewis D B and Munz W D 2002 *Surf. Coat. Technol.* **149** 217
[6] Lim S H N, McCulloch D G, Bilek M M M and McKenzie D R 2003 *J. Appl. Phys.* **93** 4283
[7] Bilek M M M, McKenzie D R, Tarrant R, Lim S H N and McCulloch D G 2002 *Surf. Coat. Technol.* **156** 136
[8] Chang C-L and Wang D-Y 2002 *Nucl. Instrum. Methods* B **194** 463
[9] Greene J E, Sundgren J-E, Hultman L, Petrov I and Bergstrom D B 1995 *Appl. Phys. Lett.* **67** 2928
[10] Kodambaka S, Israeli N, Bareno J, Swiech W, Ohmori K, Petrov I and Greene J E 2004 *Surf. Sci.* **560** 53
[11] Van Wyk G N and Smith H J 1980 *Nucl. Instrum. Methods* A **170** 433
[12] Dobrev D 1982 *Thin Solid Films* **92** 41
[13] Oh U C and Je J H 1993 *J. Appl. Phys.* **74** 1692
[14] Pelleg J, Zevin L Z and Lungo S 1991 *Thin Solid Films* **197** 117
[15] McKenzie D R and Bilek M M M 2001 *Thin Solid Films* **382** 280
[16] Stoney G G 1909 *Proc. R. Soc.* A **82** 172
[17] Perdew J P, Burke K and Ernzerhof M 1996 *Phys. Rev. Lett.* **77** 3865
[18] Hung A, Russo S P, McCulloch D G and Prawer S 2004 *J. Chem. Phys.* **120** 4890
[19] Murnaghan F D 1944 *Proc. Natl Acad. Sci.* **30** 244
[20] Nye J F 1984 *Physical Properties of Crystals: Their Representation by Tensors and Matrices* (Oxford: Clarendon)
[21] Kresse G and Furthmüller J 1996 *Phys. Rev.* B **54** 11169
[22] Perdew J P and Wang Y 1992 *Phys. Rev.* B **45** 13244
[23] Vanderbilt D 1990 *Phys. Rev.* B **41** 7892
[24] Kresse G and Hafner J 1994 *J. Phys.: Condens. Matter* **6** 8245
[25] Monkhorst H J and Pack J D 1976 *Phys. Rev.* B **13** 5188
[26] Marlo M and Milman V 2000 *Phys. Rev.* B **62** 2899
[27] Gall D, Kodambaka S, Wall M A, Petrov I and Greene J E 2003 *J. Appl. Phys.* **93** 9086
[28] Lim S H N, McCulloch D G, Bilek M M M and McKenzie D R 2003 *Surf. Coat. Technol.* **174/175** 76
[29] Bilek M M M, McKenzie D R and Moeller W 2004 *Surf. Coat. Technol.* **186** 21
[30] Ikeda S, Gilles S and Chenevier B 1998 *Thin Solid Films* **315** 257
[31] Tanaka Y, Gur T M, Kelly M, Hagstrom S B and Ikeda T 1993 *Thin Solid Films* **228** 238
[32] PalDey S and Deevi S C 2003 *Mater. Sci. Eng.* A **342** 58
[33] Musil J and Hruby H 2000 *Thin Solid Films* **365** 104
[34] Jiang C, Goto T and Hirai T 1994 *J. Mater. Sci.* **29** 669
[35] Chen K, Zhao L R, Rodgers J and Tse J S 2003 *J. Phys. D: Appl. Phys.* **36** 2725